Lawrence Berkeley National Laboratory
LBL Publications

Title
Probing Chemical Bonding in Uranium Dioxide by Means of High-Resolution X-ray Absorption Spectroscopy

Permalink
https://escholarship.org/uc/item/1nz4v051

Journal
The Journal of Physical Chemistry C, 120(51)

ISSN
1932-7447

Authors
Butorin, Sergei M
Modin, Anders
Vegelius, Johan R
et al.

Publication Date
2016-12-29

DOI
10.1021/acs.jpcc.6b09335

Copyright Information
This work is made available under the terms of a Creative Commons Attribution-NonCommercial-NoDerivatives License, availalbe at https://creativecommons.org/licenses/by-nc-nd/4.0/

Peer reviewed

eScholarship.org Powered by the California Digital Library
University of California

Probing Chemical Bonding in Uranium Dioxide by Means of High-Resolution X-ray Absorption Spectroscopy

Sergei M. Butorin,[*,†] Anders Modin,[‡] Johan R. Vegelius,[‡] Kristina O. Kvashnina,[¶,‖] and David K. Shuh[§]

†*Molecular and Condensed Matter Physics, Department of Physics and Astronomy, Uppsala University, P. O. Box 516, SE-751 20 Uppsala, Sweden*
‡*Department of Physics and Astronomy, Uppsala University, P. O. Box 516, SE-751 20 Uppsala, Sweden*
¶*The European Synchrotron, CS40220, 38043 Grenoble Cedex 9, France*
§*Chemical Sciences Division, Lawrence Berkeley National Laboratory, MS 70A1150, One Cyclotron Road, Berkeley, CA 94720, USA*
‖*Helmholtz-Zentrum Dresden-Rossendorf (HZDR), Institute of Resource Ecology, P.O. Box 510119, 01314, Dresden, Germany*

E-mail: sergei.butorin@physics.uu.se

Abstract

A systematic x-ray absorption study at the U $3d$, $4d$ and $4f$ edges of UO_2 was performed and the data were analyzed within framework of the Anderson impurity model. By applying the high-energy-resolution fluorescence-detection (HERFD) mode of x-ray absorption spectroscopy (XAS) at the U $3d_{3/2}$ edge and conducting the XAS measurements at the shallower U $4f$ levels, fine details of the XAS spectra were resolved resulting from reduced core-hole lifetime broadening. This multi-edge study enabled a far more effective analysis of the electronic structure at the U sites and characterization of the chemical bonding and degree of the $5f$ localization in UO_2. The results support the covalent character of UO_2 and do not agree with the suggestions of rather ionic bonding in this compound as expressed in some publications.

Introduction

While it has been agreed that UO_2 is a Mott-Hubbard system,[1] where the energy gap has $f-f$ character, the degree of localization/delocalization of the U $5f$ states in UO_2 is still under debate. The conclusions about the character of chemical bonding in UO_2 made by different research groups vary from ionic[2] to highly covalent[3] compound. The important characteristic in this respect is the U $5f$ occupancy (n_f) in the ground state of UO_2 that is often estimated from the electronic structure calculations or x-ray spectroscopic measurements. For example, n_f was deduced to be close to 2.0 electrons from the analysis of the resonant x-ray emission spectra[2] at the U L_3 edge of UO_2 while the analysis of the x-ray photoemission spectroscopy (XPS) data[4–6] suggested $n_f \simeq 2.3$ electrons. The latter results indicate some degree of covalency in the chemical bonding of this dioxide.

The employment of the advanced theoretical/computational formalisms, based on lo-

cal density approximation with added $5f-5f$ Coulomb interaction (LDA+U),[7,8] self-interaction corrected (SIC)-LDA,[9] LDA+DMFT (dynamical meanfield theory),[3,10] and hybrid density functional of Heyd, Scuseria, and Enzerhof (HSE)[11] to describe both the ground state and spectroscopic data of UO_2 did not lead to consensus with respect to the character of chemical bonding in general and the value of n_f in particular. The U $5f$ occupancy was calculated to be both as low as 2.0 electrons[9,10] and as high as 2.5 electrons.[3] The uncertainty calls for further studies to resolve this situation, preferably with advanced experimental methods.

An advanced technique, high-energy-resolution fluorescence-detection (HERFD) mode of x-ray absorption spectroscopy (XAS), has been recently applied for measurements at the $3d$ (M_4) edge of actinide compounds.[12–15] This has allowed for a significant improvement in experimental resolution and revealed additional structures in the XAS spectra, previously not measurable. The analysis of the newly resolved structures has enabled more accurate characterization of the chemical bonding in actinide compounds.[14,15] Another way to improve the experimental resolution has been demonstrated by conducting XAS measurements at the actinide $4f$ ($N_{6,7}$) edges.[16,17] This approach probes the unoccupied $6d$ states of actinides, similar to the measurements at the actinide $2p_{3/2}$ (L_3) edge, but the $4f$ core-hole lifetime broadening is significantly smaller,[18,19] thus allowing resolution of additional spectral structures.

In this paper, we performed a systematic study of the XAS data at multiplt uranium core level thresholds in UO_2 and estimated the degree of covalency (or n_f) in the chemical bonding in this system.

Experimental methods

The details of the measurement of the U M_4 ($3d_{3/2} \rightarrow 5f, 7p$ transitions) HERFD-XAS spectra and the UO_2- and $UO_2(NO_3)_2{\cdot}6H_2O$-sample preparation and characterization are described in Refs.[8,12] The total electron yield (TEY) spectra at U $3d$ edges were measured under conditions described in Refs.[20,21]

Experiments in the energy range of the U $N_{4,5}$ ($4d \rightarrow 5f, 7p$ transitions) and $N_{6,7}$ ($4f \rightarrow 6d, 5g$ transitions) edges of UO_2 were performed at beamline 7.0.1 of the Advanced Light Source of Lawrence Berkeley National Laboratory, employing a spherical grating monochromator.[22] U $4d$ and $4f$ XAS data were measured in the TEY mode using drain current on the sample. The incidence angle of the incoming photons was close to 90° to the surface of the samples. The monochromator resolution was set to ∼150 meV at 385 eV and to ∼400 meV at 740 eV during measurements at the U $4f$ and $4d$ edges, respectively. In this case, the UO_2 sample was powder acquired from Alfa-Aesar which was pressed in the indium substrate.

Computational details

For calculations, the Anderson impurity model[23] (AIM) was used which included the $5f$ and core d states ($3d$ or $4d$) on a single actinide ion and a filled ligand $2p$ band. The total Hamiltonian of a system can be written as

$$H = H_{AIM} + H_{FI} + H_{CF}, \qquad (1)$$

where H_{AIM} is the AIM Hamiltonian without the multiplet-coupling effects, H_{FI} represents the Coulomb, exchange and spin-orbit interactions for free actinide ion and H_{CF} describes the crystal-field splittings.

$$\begin{aligned} H_{AIM} &= \epsilon_f \sum_{\gamma} f^{\dagger}_{\gamma} f_{\gamma} + \epsilon_d \sum_{\mu} d^{\dagger}_{\mu} d_{\mu} + \sum_{n,\gamma} \epsilon_n p^{\dagger}_{n\gamma} p_{n\gamma} \\ &+ U_{ff} \sum_{\gamma>\gamma'} f^{\dagger}_{\gamma} f_{\gamma} f^{\dagger}_{\gamma'} f_{\gamma'} - U_{fc} \sum_{\gamma,\mu} f^{\dagger}_{\gamma} f_{\gamma} d^{\dagger}_{\mu} d_{\mu} \\ &+ V \sum_{n,\gamma} (p^{\dagger}_{n\gamma} f_{\gamma} + f^{\dagger}_{\gamma} p_{n\gamma}), \qquad (2) \end{aligned}$$

where ϵ_f, ϵ_d and ϵ_n are one-electron energies of actinide $5f$, core d ($3d$ or $4d$) and ligand $2p$ levels, respectively, and $f^{\dagger}_{\gamma}$, $d^{\dagger}_{\mu}$, $p^{\dagger}_{n\gamma}$ are electron creation operators at these levels with combined

indexes γ (μ) to represent the spin and orbital states of the $5f$ ($3d$ or $4d$) electrons, the index n runs over a number of discrete levels representing the ligand $2p$ band. U_{ff} denotes the $5f$-$5f$ Coulomb interaction, U_{fc} is the ($3d$ or $4d$) core hole potential acting on the $5f$ electron and V is the actinide $5f-$ligand $2p$ hybridization term.

$$\begin{aligned} H_{FI} &= \sum_{\gamma_1,\gamma_2,\gamma_3,\gamma_4} R_{ff}(\gamma_1,\gamma_2,\gamma_3,\gamma_4) f^\dagger_{\gamma_1} f^\dagger_{\gamma_2} f_{\gamma_3} f_{\gamma_4} \\ &+ \sum_{\gamma_1,\gamma_2,\mu_1,\mu_2} R_{fd}(\gamma_1,\mu_1,\mu_2,\gamma_2) f^\dagger_{\gamma_1} d^\dagger_{\mu_1} d_{\mu_2} f_{\gamma_2} \\ &+ \zeta_f \sum_{\gamma_1,\gamma_2} \langle\gamma_1|\boldsymbol{l.s}|\gamma_2\rangle f^\dagger_{\gamma_1} f_{\gamma_2} \\ &+ \zeta_d \sum_{\mu_1,\mu_2} \langle\mu_1|\boldsymbol{l.s}|\mu_2\rangle d^\dagger_{\mu_1} d_{\mu_2}, \end{aligned} \quad (3)$$

where the interactions between $5f$ electrons (R_{ff}) and a $5f$ electron and a core $3d$ or $4d$ hole (R_{fd}) are described in terms of Slater integrals (Ref.,[24] see also Ref.[25]) and spin-orbit interactions for the $5f$ and core d states are described with coupling constants ζ_f and ζ_d and matrix elements of the spin-orbit interaction $\boldsymbol{l.s}$ operator in the $5f$ and core d states.

$$H_{CF} = \sum_{\gamma,\gamma'} Q^{CF}_{\gamma\gamma'} f^\dagger_\gamma f_{\gamma'}, \quad (4)$$

where Q^{CF} is the potential provided by the crystal environment around the actinide ion which can be expanded[26] in terms of tensor operators C^k_q as

$$Q^{CF} = \sum_{k,q} B^k_q C^k_q, \quad (5)$$

where B^k_q are crystal-field parameters introduced by Wybourne.[26] The C^k_q are related to the spherical harmonics as

$$C^k_q = \sqrt{\frac{4\pi}{2k+1}} Y^k_q. \quad (6)$$

For f electrons, the terms in the expansion with $k \leq 6$ are nonzero. For cubic site-symmetry as in UO_2, only two crystal field parameters (one of rank 4 and one of rank 6) are independent. The crystal field potential can be rewritten as

$$\begin{aligned} Q^{CF} &= B^4_0[C^4_0 + \sqrt{\frac{5}{14}}(C^4_4 + C^4_{-4})] \\ &+ B^6_0[C^6_0 - \sqrt{\frac{7}{2}}(C^6_4 + C^6_{-4})]. \end{aligned} \quad (7)$$

The XAS spectra were calculated using the following equation

$$I(\omega) = \sum_m |\langle m|D_1|g\rangle|^2 \frac{\Gamma_m/\pi}{(E_m - E_g - \omega)^2 + \Gamma^2_m} \quad (8)$$

where $|g\rangle$ and $|m\rangle$ are the ground and XAS final states of the spectroscopic process with energies E_g and E_m, respectively. D is the operator for the optical dipole transition with the incident photon energy represented by ω and lifetime broadening Γ_m of the final state in terms of half-width at half-maximum (HWHM).

The required Slater integrals, spin-orbit coupling constants ζ and matrix elements were obtained with the TT-MULTIPLETS package which combines Cowan's atomic multiplet program[25] (based on the Hartree-Fock method with relativistic corrections) and Butler's point-group program,[27] which were modified by Thole,[28] as well as the charge-transfer program written by Thole and Ogasawara.

Note that in the calculations described in this section it is difficult to reproduce accurately the absolute energies (the difference with experiment is usually on the order of a few eV) so that the calculated spectra need to be uniformly shifted on the photon energy scale for comparison with experimental data. Since no significant differences in the core-hole lifetime for final states of different symmetries throughout actinide $3d$, $4d$ and $4f$ edges are expected in contrast to the actinide $5d$ edges,[29–31] a constant core-hole lifetime broadening was applied to all transitions across the entire energy range of the calculated spectrum.

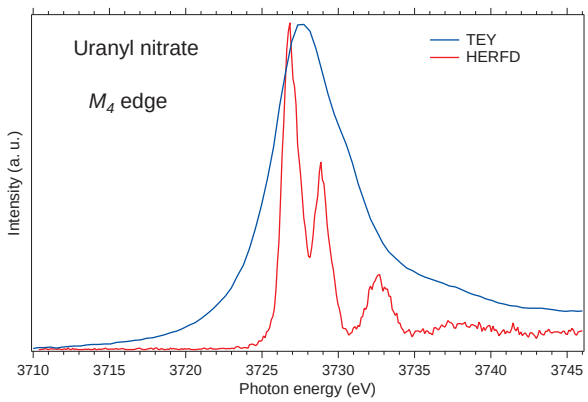

Figure 1: XAS spectra at the U M_4 edge of $UO_2(NO_3)_2{\cdot}6H_2O$ measured in the TEY (blue line) and HERFD (red line) modes.

Results and discussion

$3d$ edge

An example of the improvement of the experimental resolution, Fig. 1 displays the U M_4 XAS spectra of $UO_2(NO_3)_2{\cdot}6H_2O$ recorded in the TEY[20] and HERFD modes. The self-absorption/saturation effects are minimized in the TEY mode and therefore the TEY spectrum closely reflects the "true" absorption cross-section. This spectrum is similar to the XAS data published in Refs.[32,33] which were also measured in the TEY or direct transmission modes. The HERFD spectrum recorded by detecting the photons with an energy corresponding to the maximum of the U $M\beta$ x-ray emission line shows much narrower lines as compared to the TEY spectrum and reveals additional structures. Besides the main line, there are three structures at ∼3728.9 eV, ∼3732.6 eV and ∼3738.3 eV clearly resolved in contrast to just a high-energy shoulder in the TEY spectrum.

The main reason for the improved resolution of the HERFD-XAS spectrum is the reduced core-hole lifetime broadening. In HERFD-XAS measurements at U $M_{4,5}$ edges, the $3d$ core hole (in the final state of conventional XAS) is replaced by the $4f$ core hole in the final state of the spectroscopic process. This results in approximately four times better resolution because the $4f$ core hole lifetime broadening (full-width at half-maximum, FWHM) is estimated to be ∼0.8 eV[19] versus ∼3.2 eV for the $3d$ core hole.

In principle, there is some difference between the $3d^95f^{n+1}$ and $4f^{13}5f^{n+1}$ multiplets in terms of the number of states and interactions between the electrons, however, the constant energy detection of emitted photons puts an additional restriction on transitions contributing to the spectra. Although, one might expect deviations in the shape of the HERFD spectra from the x-ray absorption cross-sections, it has already been shown by calculations[34,35] for the $2p-4f$ quadrupole transitions in Dy_2O_3 that the difference between the HERFD-XAS and conventional XAS (with reduced broadening) spectra is not significant when only the emitted photons with an energy of the maximum of the corresponding $2p-3d$ x-ray emission line are counted. No significant difference has been found between HERFD-XAS and conventional XAS (with reduced broadening) at the U M_4 edge of the U(V) systems.[15] In any case, the expected differences between the $3d^95f^{n+1}$ and $4f^{13}5f^{n+1}$ multiplets are small compared to the resolution achieved by the HERFD-XAS technique in our measurements.

In Fig. 2, the U M_4 HERFD-XAS spectrum of UO_2 is compared with results of the atomic- and crystal-field multiplet and AIM calculations for the U(IV) system. Within the atomic- and crystal-field multiplet theory, the spectra were calculated for transitions between $5f^2$ and $3d^95f^3$ configurations. It is interesting in the atomic-multiplet approach for the $^3H_4$ ground state that the calculations already produce all of the structures observed in the experimental spectrum, even a small structure at ∼3733 eV. While the electrostatic $F^k(5f,5f)$ and $F^k(3d,5f)$ Slater integrals were scaled down to 80% of their Hartree-Fock values in these calculations, the exchange $G^k(3d,5f)$ integrals were reduced to 50% to lessen the intensity of the shoulder at around 3726.8 eV with respect to the main peak to provide better agreement with the experiment (see a comparison with the spectrum [blue dashed curve] calculated for the "standard" G^k reduction to 80% in Fig. 2). Such a significant reduction indicates weaker influence of the core hole, probably orig-

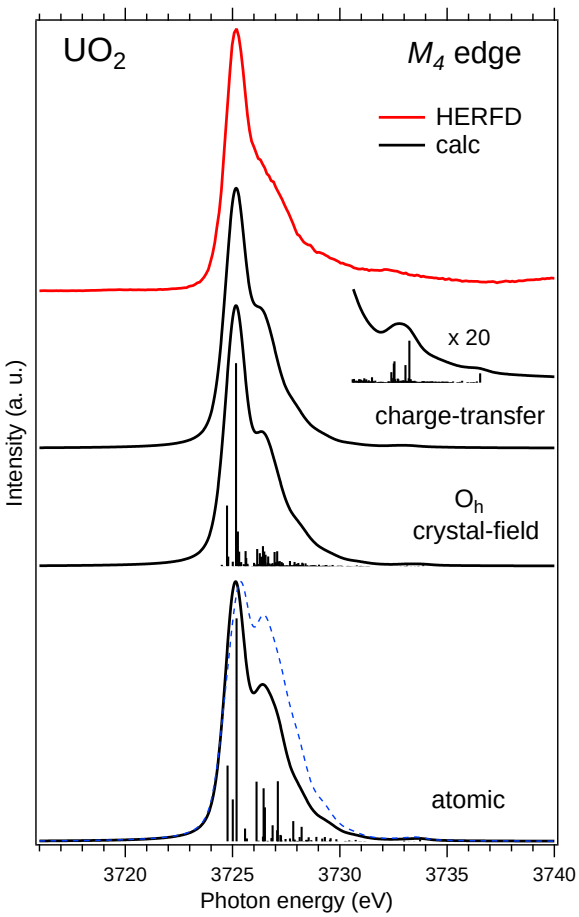

Figure 2: Experimental (Ref.[12]) and calculated XAS spectra at the U M_4 edge of UO_2. The spectra are calculated using atomic and crystal-field multiplet theory for the U^{4+} ion and Anderson impurity model, respectively. The blue dashed line represents the results of atomic multiplet calculations with G^k integrals reduced to 80% of their Hartree-Fock values (see text).

inating from an increased number of $5f$ electrons, as compared to the Th case.[14] Nevertheless, the spectrum calculated within the atomic multiplet approach is notably wider than the experimental one.

Using the crystal-field multiplet theory with local cubic (O_h) symmetry for the U(IV) ion and taking into account the U $5f$–O $2p$ hybridization within AIM framework improves the agreement with experiment in terms of a further decrease in the intensity of the shoulder at ~3726.8 eV and further reduction in the overall width of the calculated spectrum. In the AIM, the ground (final) state of the U(IV) system was described as a mixture of the $5f^2$ and $5f^3\underline{v}^1$ ($3d^95f^3$ and $3d^95f^4\underline{v}^1$) configurations. The contributions of the $5f^4\underline{v}^2$ configuration in the ground state and the $3d^95f^5\underline{v}^2$ configuration in the final state are expected to be small. For UO_2, the U $5f$–O $2p$ charge-transfer is the dominant process in contrast to ThO_2[14] since the U $5f$ states are at the bottom of the conduction band (see the results of LDA+U calculations, e.g., Refs.[7,8]).

In the limit of $V \to 0$, the difference between the configuration averaged energies for the ground state can be written as $E(5f^3\underline{v}^1) - E(5f^2) = \Delta$ (where $\Delta \equiv \epsilon_f - \epsilon_n$, with ϵ_n corresponding to the center of the O $2p$ band) which is the so-called charge-transfer energy. For the final state, this difference is $E(3d^95f^4\underline{v}^1) - E(3d^95f^3) = \Delta + U_{ff} - U_{fc}$. The spectra displayed in Fig. 2 were calculated with the following model parameter values: $B_0^4 = -0.93$ eV and $B_0^6 = 0.35$ eV, $\Delta = 6.0$ eV, $U_{ff} = 4.5$ eV, $U_{fc} = 6.0$ eV, $V_g = 1.2$ eV and $V_m = 1.0$ eV. The strength of the Coulomb interaction between $5f$ electrons in UO_2 has been studied and discussed in many publications and the value of U_{ff} applied here corresponds well to the previously discussed values. Furthermore, the same values of U_{ff} and Δ and a similar value of hybridization term V were used to calculate the U $4f$ XPS spectrum[6] of UO_2. Taking into account the U $5f$–O $2p$ hybridization results in an appearance of some spectral weight/intensity at energies higher than 3734 eV. The intensity of this charge-transfer satellite is fairly weak because of a relatively large Δ, nevertheless it may explain the extended tail observed in the experimental spectrum at corresponding energies.

Our calculations show that the $5f^3\underline{v}^1$ contribution in the ground state amounts to 24%, thus resulting in a U $5f$ occupancy of 2.24 electrons. This result agrees with estimations of the U $5f$ occupancy in the ground state of UO_2 made in a number of publications where x-ray spectroscopic data were calculated. The calculations of the U $4f$ XPS spectrum using AIM[6] employing similar values for model parameters resulted in the U $5f$ occupancy value of 2.26 electrons and using the *ab-initio* embedded-UO_8-cluster approach[38] yielded 2.35 electrons. The hybrid density functional the-

ory method[11] employed for a description of the valence-band photoemission data produced 2.36 electrons. Only the local-density approximation combined with the dynamical mean-field theory (LDA+DMFT) method[3] used to calculate both core U $4f$ and valence-band photoemission spectra of UO_2 yielded U $5f$ occupancy of 2.5 electrons in the ground state. The latter value of n_f seems somewhat large for a Mott-Hubbard system with relatively large Δ, especially in comparison with highly-covalent CeO_2 where Ce is determined to gain about 0.5 $4f$-electrons from the strong Ce $4f-$O $2p$ hybridization and charge transfer. Furthermore, in these LDA+DMFT calculations, U_{ff} was set to be larger than U_{fc} which is usually the other way around for the case of core-level photoemission spectroscopy.

The crystal-field parameter values $B_0^4 = -0.93$ eV and $B_0^6 = 0.35$ eV are in good agreement with those derived from the INS experiment,[39] but differ significantly from the B_0^4 value given in Ref.[40] However, the value from Ref.[40] seems to be overestimated because the calculated energy separation of the lowest excited states of the $5f^2$ multiplet from the ground state is somewhat too large when compared with experiment[39] and LDA+DMFT calculations.[3] Table 1 compares the lowest excited states of the U $5f$ multiplet obtained from our AIM calculations for a cubic crystal-field environment with those detected by INS under conditions above the ordering temperature. The agreement between theory and experiment is fairly good. The inclusion of the U $5f-$O $2p$ hybridization in the calculations was an important factor for obtaining such agreement.

$4d$ edges

Utilizing the shallow electron core levels of actinides, one might expect an improvement in resolution for x-ray absorption spectra resulting from a reduced core-hole lifetime broadening but unfortunately it is not the case for the $4d$ edges of actinides. It has been determined to be even larger (∼4.2 eV FWHM)[41] than the $3d$ core-hole lifetime broadening. Therefore, the U $N_{4,5}$ x-ray absorption spectrum shown in

Table 1: Lowest states of the U $5f$ multiplet (meV) calculated for cubic crystal-field environment within Anderson impurity model compared to those measured in the inelastic neutron scattering (INS)[39] experiments under conditions above the ordering temperature.

State	Experiment (INS)	Calculations
Γ_5		0
Γ_3	150	155
Γ_4	170	178

Fig. 3 recorded in the TEY mode appears as two broad, nearly structureless lines at around 735.3 eV and 776.7 eV, which represent the spin-orbit $4d_{5/2}$ and $4d_{3/2}$ pair, respectively. The broad structure observed for the range of energies between ∼749 and ∼758 eV represents transitions to the continuum (probably p-like) states. The model does not include transitions to the continuum and our calculations do not take these transitions into account.

However, if high-energy resolution was attainable, one would observe that the shapes of the N_5 and N_4 edges are different. That is a direct consequence of the interaction of the $5f$ electrons with the $4d$ core hole in the final state of the spectroscopic process. This is clearly seen when comparing the experimental data with the results of calculations using the atomic multiplet, crystal-field multiplet theory and AIM for the U(IV) ion in Fig. 3. In the atomic and crystal-field approach, the spectra were calculated for transitions between $5f^2$ and $4d^9 5f^3$ configurations. For the calculated spectra, shown in Fig. 3, the F^k integrals were reduced to 80% while the G^k integrals were reduced to 65% as in calculations for the U $4f$ edges (see below). However, in contrast to the situation for the M_4 edge, the spectral shapes at the $4d$ edges are little affected by G^k scaling to 50% versus "standard" scaling to 80%, probably due to (in general) significantly smaller values of the G^k integrals at the $4d$ edges compared to the $3d$ edges.[40] The crystal-field parameters were set to the same values as in the calculations for the U M_4 edge.

In the AIM calculations, the final state of the

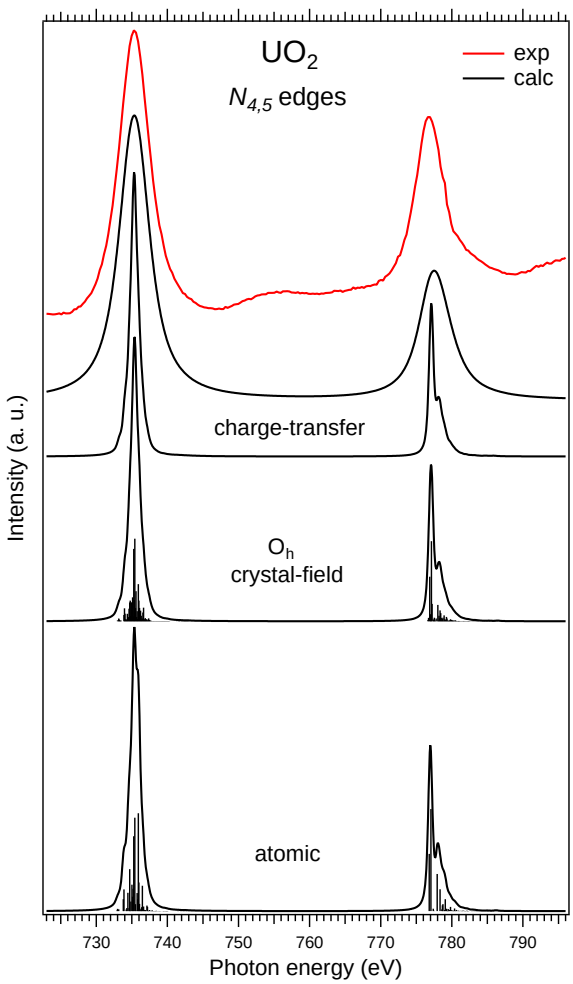

Figure 3: Experimental and calculated XAS spectra at the U $N_{4,5}$ edges of UO_2. The spectra are calculated using atomic and crystal-field multiplet theory for the U^{4+} ion and Anderson impurity model, respectively.

system was described as a mixture of $4d^9 5f^3$ and $4d^9 5f^4 \underline{\upsilon}^1$ configurations while the description of the ground state and the values of the model parameters were kept the same as in the calculations for the U M_4 edge. To more easily identify the differences between the U N_5 and N_4 edges, the calculated spectra were only slightly broadened. While already the atomic multiplet calculations demonstrate a significant contrast in the shape between the U(IV) N_5 and N_4 edges, switching on the crystal field and the U $5f-$O $2p$ hybridization adds to the shape changes.

An important quantity discussed in connection with the $4d$ edges of actinides is the branching ratio of the N_5 and N_4 lines (see e.g., Refs.[2,30,42]) as a characteristic of the actinide oxidation state and $5f$ count n_f. The branching ratio is defined as $I_{5/2}/(I_{5/2} + I_{3/2})$, where I is the integrated intensity of a line. A gradual decrease of the relative N_4 intensity and a corresponding increase of the branching ratio were demonstrated on going from the $n_f = 1$ system (Th metal) to the $n_f = 6$ system (Am metal) with reference to the nominal oxidation state/$5f$ population. However, there is disagreement on whether the branching ratio is sensitive to the crystal field symmetry and the covalency of the chemical bonds in uranium compounds, particularly for UO_2. The contradictory conclusions were made based on results of electron-energy-loss spectroscopy[42] and conventional XAS.[2]

Our calculations do not reveal a change in the branching ratio on going from the pure atomic-multiplet theory to taking into account the crystal-field interaction and the U $5f-$O $2p$ hybridization. Even the admixture of an extra 0.24 $5f$-electrons accounting for the chemical-bonding covalency and U $5f-$O $2p$ charge-transfer in the ground state and configuration mixing in the final state do not significantly affect the branching ratio. This ratio was found to be 0.68 which is in good agreement with experiment.[2]

The AIM spectrum which takes into account all the crystal-field multiplet effects and the U $5f-$O $2p$ hybridization was also fully broadened to account for the $4d$ core-hole lifetime and the experimental resolution, and is compared with the measured spectrum in Fig. 3. One can see that for real broadenings in conventional XAS measurements at the actinide $4d$ edges it is very difficult to observe shape differences between the N_5 and N_4 lines. At the same time, the sensitivity of their branching ratio to oxidation state remains an issue to explore further.

$4f$ edges

In contrast to the actinide $4d$ XAS edges, the improvement in spectral resolution moving to the shallower actinide $4f$ XAS thresholds is achieved from a significantly reduced core-hole

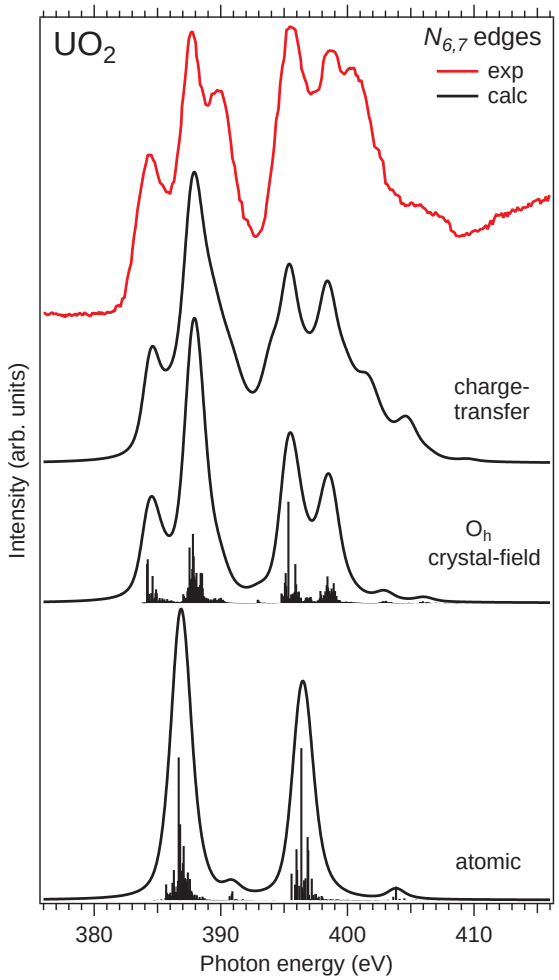

Figure 4: Experimental and calculated XAS spectra at the U $N_{6,7}$ edges of UO_2. The spectra are calculated using atomic and crystal-field multiplet theory for the U^{4+} ion and Anderson impurity model, respectively.

lifetime broadening,[18,19] thus providing more detailed information about the unoccupied $6d$ states of actinides compared to normal XAS experiments at the actinide L_3 edge.

In Ref.,[17] the XAS spectra of AnO_2 (An = U, Np, Pu) at the An $N_{6,7}$ edges were compared with the LDA+U-calculated unoccupied An $6d$ density of states. Although the results of the LDA+U calculations describe all the observed spectral structures, the spectral shapes are not accurately reproduced especially the differences in shape between the N_7 and N_6 edges. In particular for UO_2 (see Fig. 4), the first peak (at ∼384.4 eV) of the N_7 edge which is not so strong becomes the most intense structure (at ∼395.5 eV) in the N_6 edge.

We have employed an alternative, many-body (multiplet coupling) approach based on AIM to describe the XAS spectra at the actinide $4f$ edges in this research. Fig. 4 compares the results of atomic, crystal-field multiplet and AIM theories for the U(IV) system with the experimental XAS data obtained at the U $N_{6,7}$ edges of UO_2. The atomic and crystal-field multiplet calculations were performed for the transitions between the $5f^2$ (ground state) and $4f^{13}5f^26d^1$ (final state) configurations. The F^k Slater integrals were reduced to 80% of their Hartree-Fock values while the G^k integrals were reduced to 65% (see below). In the crystal-field multiplet calculations, the cubic (O_h) crystal field was applied to both U $5f$ and $6d$ shells with parameters set to $B_0^4 = -0.93$ eV, $B_0^6 = 0.35$ eV ($5f$ shell), and $10Dq = -3.00$ eV ($6d$ shell), respectively.

It is clear from Fig. 4 that the atomic-multiplet theory fails to describe the U $N_{6,7}$ XAS spectrum of UO_2, while the crystal-field multiplet calculations fairly-well reproduce the major difference between the U N_7 and U N_6 edges, i.e., the first peak at ∼395.5 eV is the most prominent structure of the N_6 edge contrasting to the N_7 edge where the second peak at ∼387.7 eV is the strongest. The splittings between the peaks at ∼384.4 eV and ∼387.7 eV in the N_7 edge and between the peaks at ∼395.5 eV and ∼398.6 eV in the N_6 edge directly depend on the $10Dq$ parameter for the U $6d$ shell and is well-reproduced for $10Dq = -3.00$ eV. This value is somewhat different from those derived in Refs.[8,17] because it describes the "bare" splitting between the e_g and t_{2g} states without the effects of the $6d$ hybridization.

It turns out that the U $N_{6,7}$ XAS spectral structures of UO_2 between 402.5 eV and 410 eV result from the exchange interaction between core and valence electrons. This is easily revealed by scaling the G^k integrals in the calculations so that the positions of the structures move towards higher energies with increasing G^k values. Therefore, the energy positions of these structures observed in the experimental spectrum put additional constraints on and help to accurately determine the strength of the exchange interaction. As in case of the

HERFD-XAS data at the U $3d$ edge of UO_2, a significant reduction of the G^k integrals is required for a proper description of the experimental XAS data at the U $4f$ edges of UO_2.

Despite a significant improvement in the description of the experimental data, the crystal-field multiplet theory does not correctly reproduce the ∼390.1-eV and ∼401.0-eV peaks in the measured U $N_{6,7}$ XAS spectrum of UO_2. Although the splitting between the e_g and t_{2g} orbitals is introduced in the U $6d$ shell, the actual $6d$ band shape is not modeled in this case. This is one of the possible reasons for the discrepancy between calculations and experiment. Another reason is the importance of the U $5f$−O $2p$ hybridization and charge-transfer in UO_2.

The results of the AIM calculations for the U(IV) system that take into account the U $5f$−O $2p$ hybridization and charge-transfer do reveal an enhanced spectral weight ("extra-structures") at the energies around 390.1 and 401.0 eV (see Fig. 4), although the intensities are not as large as in the experimental spectrum. Since in this case a core hole at the U site is created in the U $4f$ level instead of the $3d$ ($4d$) level and an electron is excited into the U $6d$ states, the model Hamiltonian was accordingly modified.

In H_{AIM}, ϵ_d and $d^\dagger_\mu$ were replaced with a one-electron energy, ϵ_c, and the electron creation operator $c^\dagger_\alpha$ for the $4f$ level, respectively. Two extra terms were added to account for the $5f-6d$ Coulomb interaction (U_{fd}) and the $4f$ core-hole potential acting on the $6d$ electron (U_{dc}), such as

$$U_{fd}\sum_{\gamma,\lambda} f^\dagger_\gamma f_\gamma a^\dagger_\lambda a_\lambda - U_{dc}\sum_{\lambda,\alpha} a^\dagger_\lambda a_\lambda c^\dagger_\alpha c_\alpha$$

where $a^\dagger_\lambda$ is an electron creation operator in the $6d$ level and λ (α) represents the spin and orbital states of the $6d$ ($4f$) electrons. The importance of the inclusion of such terms has been demonstrated for the description of the Ce L_3 XAS spectrum of CeO_2.[43]

In H_{FI} (equation 3), the $3d$ ($4d$) spin-orbit coupling and Slater integrals of the $3d(4d)-5f$ interaction were replaced with the $4f$ spin-orbit coupling and $4f-5f$ and $4f-6d$ interaction integrals, respectively. In addition, the $6d$ spin-orbit coupling and $5f-6d$ interaction integrals were taken into account. In H_{CF}, the crystal-field term for the $6d$ shell was included which can be characterized by the $10Dq$ parameter under O_h symmetry.

While the ground state was the same as in the AIM calculations of the XAS spectra of UO_2 at the U $3d$ and $4d$ edges, the final state of the XAS process at the U $4f$ edges was described by a mixture of the $4f^{13}5f^26d^1$ and $4f^{13}5f^3\underline{v}^16d^1$ configurations. In the limit of $V\rightarrow 0$, the difference between the configuration averaged energies for the final state can be expressed as $E(4f^{13}5f^3\underline{v}^16d^1)-E(4f^{13}5f^26d^1)=\Delta-U_{fc}-U_{dc}+U_{fd}$ (see Ref.[43]). The values of the AIM parameters were the same as those used for calculations of the XAS spectra of UO_2 at the U $3d$ and $4d$ edges, except for the V_m value which was set to $V_m = 0.6$ eV. The $(U_{dc}-U_{fd})$ value was found to affect the energy positions of the "extra-structures", discussed above, and was eventually set to $U_{dc}-U_{fd}=2.0$ eV to provide better agreement with respect to experimental energy (measured structures around 390.1 and 401.0 eV). A similar $(U_{dc}-U_{fd})$ value was derived for ThO_2 in Ref.[14] and $U_{dc}-U_{fd}=1.0$ eV was estimated for Ce L_3 XAS edge of CeO_2 in Ref.[43]

From comparison between the results of the calculations based only on crystal-field theory and the AIM calculations, which take into account the U $5f$−O $2p$ charge-transfer, it is clear that most of the spectral weight at ∼390.1 eV and ∼401.0 eV originates from the transitions to the states of the $4f^{13}5f^3\underline{v}^16d^1$ configuration. At the same time, a comparison of the experimental spectra with the results of LDA+U calculations in Ref.[17] suggests that the ∼390.1-eV and ∼401.0-eV structures correspond to the transitions to the t_{2g}-derived states. However, the LDA+U calculations do not really distinguish between contributions from different electronic configurations. In this situation, the polarization-dependent and temperature-dependent XAS measurements on a single crystal of UO_2 (in particular at low temperatures when there is a crystal-structure distortion)

could help in establishing the nature of the ∼390.1-eV and ∼401.0-eV structures.

Conclusions

A systematic XAS study of UO_2, involving both advanced experimental methods, such as HERFD-XAS, and measurements at shallower U core levels in combination with the AIM calculations, has helped to better evaluate the chemical bonding and the degree of the $5f$ localization in this oxide. The AIM simulations of the data produced the n_f value of 2.24 electrons. The results of our study firmly support the significant degree of covalency of chemical bonding in UO_2 despite the suggestions of rather ionic character of this oxide expressed by some researchers.

Acknowledgement This research was supported by the Director, Office of Science, Office of Basic Energy Sciences, Division of Chemical Sciences, Geosciences, and Biosciences Heavy Element Chemistry program (D.K.S) and the Advanced Light Source is supported by the Director, Office of Science, Basic Energy Sciences; both of the US Department of Energy at Lawrence Berkeley National Laboratory under Contract DE-AC02-05CH11231.

References

(1) Dudarev, S. L.; Nguyen Manh, D.; Sutton, A. P. Effect of Mott-Hubbard correlations on the electronic structure and structural stability of uranium dioxide. *Phil. Mag. B* **1997**, *75*, 613-628.

(2) Tobin, J. G.; Yu, S.-W.; Booth, C. H.; Tyliszczak, T.; Shuh, D. K.; van der Laan, G.; Sokaras, D.; Nordlund, D.; Weng, T.-C.; Bagus, P. S. Oxidation and crystal field effects in uranium. *Phys. Rev. B* **2015**, *92*, 035111.

(3) J. Kolorenč, J.; Shick, A. B.; Lichtenstein, A. I. Electronic structure and core-level spectra of light actinide dioxides in the dynamical mean-field theory. *Phys. Rev. B* **2015**, *92*, 085125.

(4) Gunnarsson, O.; Li, T. C. Resonance photoemission for f-electron systems. *Phys. Rev. B* **1987**, *36*, 9488-9499.

(5) Gunnarsson, O.; Sarma, D. D.; Hillebrecht, F. U.; Schönhammer, K. Electronic structure of the light actinide oxides from electron spectroscopy. *J. Appl. Phys.* **1988**, *63*, 3676-3679.

(6) Kotani, A.; Ogasawara, H. Theory of core-level spectroscopy in actinide systems. *Physica B* **1993**, *186-188*, 16-20.

(7) Modin, A.; Suzuki, M.-T.; Vegelius, J.; Yun, Y.; Shuh, D. K.; Werme, L.; Nordgren, J.; Oppeneer, P. M.; S. M. Butorin, S. M. $5f$-Shell correlation effects in dioxides of light actinides studied by O $1s$ x-ray absorption and emission spectroscopies and first-principles calculations. *J. Phys.: Condens. Matter* **2015**, 27, 315503.

(8) Kvashnina, K. O.; Kvashnin, Y. O.; Vegelius, J. R.; Bosak, A.; Martin, M.; Butorin, S. M. Sensitivity to actinide doping of uranium compounds by resonant inelastic x-ray scattering at uranium L_3 edge. *Anal. Chem.* **2015**, *87*, 8772-8780.

(9) Petit, L.; Svane, A.; Szotek, Z.; Temmerman, W. M.; Stocks, G. M. Electronic structure and ionicity of actinide oxides from first principles. *Phys. Rev. B* **2010**, *81*, 045108.

(10) Yin, Q.; Kutepov, A.; Haule, K.; Kotliar, G.; Savrasov, S. Y.; Pickett, W. E. Electronic correlation and transport properties of nuclear fuel materials. *Phys. Rev. B* **2011**, *84*, 195111.

(11) Roy, L. E.; Durakiewicz, T.; Martin, R. L.; Peralta, J. E.; Scuseria, G. E.; Olson, C. G.; Joyce, J. J.; Guziewicz, E. Dispersion in the Mott insulator UO_2: A comparison of photoemission spectroscopy and

screened hybrid density functional theory. *J. Comput. Chem.* **2008**, *29*, 2288-2294.

(12) Kvashnina, K. O.; Butorin, S. M.; Martin, P.; Glatzel, P. Chemical state of complex uranium oxides. *Phys. Rev. Lett.* **2013**, *111*, 253002.

(13) Kvashnina, K. O.; Kvashnin, Y. O.; Butorin, S. M. Role of resonant inelastic x-ray scattering in high-resolution core-level spectroscopy of actinide materials. *J. Electron Spectrosc. Relat. Phenom.* **2014**, *194*, 27-36.

(14) Butorin, S. M., Kvashnina, K. O.; Vegelius, J. R.; Meyer, D.; Shuh, D. K. High-resolution x-ray absorption spectroscopy as a probe of crystal-field and covalency effects in actinide compounds. *PNAS* **2016**, *113*, 8093-8097.

(15) Butorin, S. M., Kvashnina, K. O.; Smith, A. L.; Popa, K.; Martin, P. M. Crystal-field and covalency effects in uranates: An x-ray spectroscopic study. *Chem. Eur. J.* **2016**, *22*, 9693-9698.

(16) Tobin, J. G., Yu, S.-W. Orbital specificity in the unoccupied states of UO_2 from resonant inverse photoelectron spectroscopy. *Phys. Rev. Lett.* **2011**, *107*, 167406.

(17) Butorin, S. M.; Modin, A.; Vegelius, J. R.; Suzuki, M.-T.; Oppeneer, P. M.; Andersson, D. A.; Shuh, D. K. Local symmetry effects in actinide $4f$ x-ray absorption in oxides. Anal. Chem. 88, 4169-4173 (2016).

(18) Mårtensson, N.; Malmqvist, P.-A.; Svensson, S.; Johansson, B. The electron spectrum of UF_6 recorded in the gas phase. *J. Chem. Phys.* **1983**, *80*, 5458-5464.

(19) Fuggle J. C.; Alvarado S. F. Core-level lifetimes as determined by x-ray photoelectron spectroscopy measurements. *Phys. Rev. A: At., Mol., Opt. Phys.* **1980**, *22*, 1615-1624.

(20) Butorin, S. M. Resonant inelastic x-ray scattering as a probe of optical scale excitations in strongly electron-correlated systems: quasi-localized view. *J. Electron Spectros. Rel. Phenom.* **2000**, *110-111*, 213-233.

(21) Zatsepin, D. A.; Butorin, S. M.; Mancini, D.-C.; Ma, Y.; Miyano, K. E.; Shuh, D. K.; Nordgren, J. Strong anisotropy of resonant inelastic x-ray scattering from charge-transfer excitations in UO_3. *J. Phys.: Condens. Matter* **2002**, *14*, 14, 2541-2546.

(22) Warwick, T.; Heimann, P.; Mossessian, D.; McKinney, W.; Padmore, H. Performance of a high resolution, high flux density SGM undulator beamline at the ALS. *Rev. Sci. Instrum.* **1995**, *66*, 2037-2040.

(23) Anderson, P. W. Localized magnetic states in metals. *Phys. Rev. B* **1961**, *124*, 41-53.

(24) Slater, J. C. The theory of complex spectra. *Phys. Rev.* **1929**, *34*, 1293-1322.

(25) Cowan, R. D. *Theory of Atomic Structure and Spectra* (University of California Press, Berkeley, 1981).

(26) Wybourne, B. G. *Spectroscopic Properties of Rare Earths*, Wiley, New York, 1963.

(27) Butler, P. H. *Point Group Symmetry Applications: Methods and Tables* (Plenum Press, New York, 1981).

(28) Thole, B. T.; van der Laan, G.; Butler, P. H. Spin-mixed ground state of Fe phthalocyanine and the temperature-dependent branching ratio in x-ray absorption spectroscopy. *Chem. Phys. Lett.* **1988**, *149*, 295-299.

(29) Ogasawara, H.; Kotani, A.; Thole, B. T. Calculation of magnetic x-ray dichroism in $4d$ and $5d$ absorption spectra of actinides. *Phys. Rev. B* **1991**, *44*, 2169-2181.

(30) Moore, K. T.; van der Laan, G. Nature of the $5f$ states in actinide metals. *Rev. Modern Phys.* **2009**, *81*, 235-298.

(31) Butorin, S. M. Resonant inelastic soft x-ray scattering spectroscopy of light-actinide materials. In *Actinide Nanoparticles Research*; Kalmykov, S. N., Denecke, M. A., Eds.; Springer Science: Heidelburg, Germany, 2011; pp 63-104.

(32) Petiau, J.; Calas, G.; Petitmaire, D.; Bianconi, A.; Benfatto, M.; Marcelli, A. Delocalized versus localized unoccupied 5f states and the uranium site structure in uranium oxides and glasses probed by x-ray-absorption near-edge structure. *Phys. Rev. B* **1986**, *34*, 7350-7361.

(33) Dodge, C. J.; Francis, A. J.; Lu, F.; Halada, G. P.; Kagwade, S. V.; Clayton, C. R. Speciation of uranium after microbal action by XANES and XPS. *Mat. Res. Soc. Symp. Proc.* **1993**, *307*, 89-93.

(34) Tanaka, S.; Okada, K.; Kotani, A. Resonant x-ray emission spectroscopy in Dy compounds. *J. Phys. Soc. Jpn.* **1994**, *63*, 2780-2787.

(35) Butorin, S. M., Kvashnina, K. O.; Prieur, D.; Rivenet, M.; Martin, P. M. Characteristics of chemical bonding of pentavalent uranium in La-doped UO_2. *Chem. Comm.* in press, DOI: 10.1039/c6cc07684j.

(36) Gunnarsson, O.; Jepsen, O. Configuration dependence of hopping matrix elements in the Anderson model. *Phys. Rev. B* **1988**, *38*, 3568-3571.

(37) Sugar, J. Potential-Barrier Effects in Photoabsorption. II. Interpretation of photoabsorption resonances in lanthanide metals at the $4d$-electron threshold. *Phys. Rev. B* **1972**, *5*, 1785-1792.

(38) Bagus, P. S.; Nelin, C. J.; Ilton, E. S. Theoretical modeling of the uranium 4f XPS for U(VI) and U(IV) oxides. *J. Chem. Phys.* **2013**, *139*, 244704.

(39) Nakotte, H.; Rajaram, R.; Kern, S.; McQueeney, R. J.; Lander, G. H.; Robinson, R. A. Crystal fields in UO_2 - revisited. *J. Phys.: Conf. Series* **2010**, *251*, 012002.

(40) Ramanantoanina, H.; Kuri, G.; Daulb, C.; Bertsch, J. Core electron excitations in U^{4+}: modelling of the $nd^{10}5f^2 \rightarrow nd^9 5f^3$ transitions with n = 3, 4 and 5 by ligand field tools and density functional theory. *Phys. Chem. Chem. Phys.* **2016**, *18*, 19020-19031.

(41) Raboud, P.-A.; Dousse, J.-Cl.; Hoszowska, J.; Savo,y I. L_1 to N_5 atomic level widths of thorium and uranium as inferred from measurements of L and M x-ray spectra. *Phys. Rev. A* **2000**, *61*, 012507.

(42) Moore, K. T.; van der Laan, G.; Haire, R. G.; Wall, M. A.; Schwartz, A. J. Oxidation and aging in U and Pu probed by spin-orbit sum rule analysis: Indications for covalent metal-oxide bonds. *Phys. Rev. B* **2006**, *73*, 033109.

(43) Kotani, A.; Jo, T.; Parlebas, J. C. Many-body effects in core-level spectroscopy of rare-earth compounds. *Adv. Phys.* **1988**, *37*, 37-85.

TOC Graphic

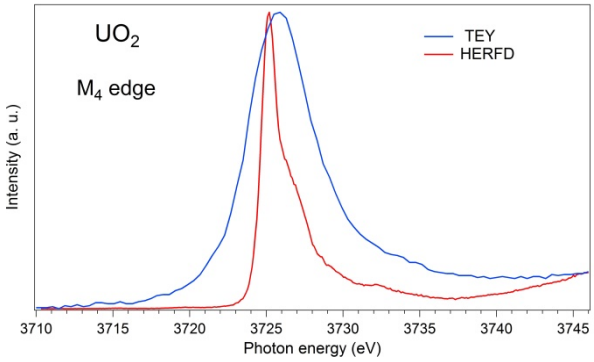
UO2
M4 edge
TEY
HERFD
Intensity (a. u.)
3710
3715
3720
3725
3730
3735
3740
3745
Photon energy (eV)